Joint Centre for Mesoscale Meteorology, Reading, UK

The dry intrusion and its effect on the frontal, cloud and precipitation structure of extratropical cyclones

K. A. Browning

Internal Report No. 68

June 1997

Met Office Joint Centre for Mesoscale Meteorology Department of Meteorology
University of Reading PO Box 243 Reading RG6 6BB United Kingdom
Tel: +44 (0)118 931 8425 Fax: +44 (0)118 931 8791
www.metoffice.com

Designed and produced by the Met Office © Crown copyright 2001 01/0240 The Met Office logo is a registered trademark.

The dry intrusion and its effect on the frontal, cloud and precipitation structure of extratropical cyclones

K.A. Browning

Text of invited special lecture at the Spring Conference
of the Meteorological Society of Japan,
University of Tsukuba, 22 May 1997

The dry intrusion and its effect on the frontal, cloud and precipitation structure of extratropical cyclones

K. A. Browning
Joint Centre for Mesoscale Meteorology,
Department of Meteorology, University of Reading,
P O Box 240, Reading, RG6 6FN, UK.

Abstract

The dry intrusion is a coherent region of air descending from near tropopause-level. It often has a clear signature in satellite imagery, especially in the water vapour channel where it is seen as a 'dark zone'. The dry intrusion is an indication of upper-level forcing. If it approaches a low-level baroclinic zone, rapid cyclogenesis may be expected to ensue. The leading edge of a dry intrusion is marked by the cold front. At an ana-cold front the dry intrusion mainly undercuts rearward-ascending warm air. At a kata-cold front it overruns the warm air to produce an upper cold (θ_w)front in advance of the surface cold front.Dry intrusions are usually associated with the generation of potential instability and its eventual release as showers or thunderstorms. Identification of dry intrusions provides the forecaster with additional evidence that is helpful when issuing severe weather warnings. The identification of dry intrusions can also form the basis of methods for validating NWP models. Through their relationship to high potential vorticity, dry intrusions provide guidance for bogussing NWP models in situations of potentially severe weather. This article provides an introduction to the structure and behaviour of dry intrusions and their relationship to other aspects of extratropical cyclones.

1. Introduction

In considering the structure of cyclones it is natural to think first in terms of moist ascent and cloud: after all, we know that latent heating plays a major role in cyclogenesis. Yet this is only half the picture. In this article we focus instead on the very dry air which often comes down to low levels near cyclones. Although reascending in places close to the cyclone centre, this air will normally have had a history of descent, the driest parts having been close to the tropopause upstream 2 days earlier. This is portrayed vividly in Figure 1, drawn as long ago as 1964 by the meteorologist-cum-artist E.F. Danielsen.

Danielsen's visualisation shows trajectories of air descending within a 3-D isentropic surface. They originate from the vicinity of a newly-developing tropopause fold and fan out as they descend toward the ground behind the cold front. Analyses by Wernli (1995) suggest that some of the cyclonic trajectories originate within the stratosphere but that most of them probably originate just on the tropospheric side of the fold. As discussed in Section 3, some of this dry air undercuts warm air ahead of it whilst other parts of the dry airstream closer to the cyclone centre overrun it to produce distinctly different frontal structures.

The exact configuration of these dry-air trajectories varies from case to case. Thorncroft et al (1993) have defined two archetypes in which either the cyclonic or the anticyclonic flow predominates depending on whether the ambient zonal shear is cyclonic or anticyclonic. It is the entire dry flow, consisting of all the trajectories in the isentropic surface in Figure 1 plus similar trajectories within adjacent isentropic surfaces, that constitutes the dry intrusion as we define it in this article. Although part of the dry intrusion is characterised by stratospheric air with high potential vorticity (PV $\geq$ 2 pv units), as noted above, this constitutes only a rather small proportion of the overall dry intrusion (see Section 5). A particularly important property of the dry intrusion is the low wet-bulb potential temperature (θ_w) of parts of it. The effect this has in generating potential instability and convection is discussed in Sections 4 and 6.

The identification of the dry intrusion as a significant entity associated with cyclone development has come to prominence through its association with a characteristic signature in satellite imagery. After the onset of cyclogenesis it can be seen as a dry slot in the water vapour (WV), infrared (IR) and, sometimes, in the visible (VIS) channel. As shown in Figure 2 the dry slot is sandwiched between a high-topped polar-front cloud-band on one side and an often slightly lower cloud feature, known as a cloud head, on the cold-air side. We elaborate on the relationship of the dry intrusion to the airflows in these cloudy regions in Section 2.

Prior to the development of the dry slot, the dry intrusion is not detectable in the IR or VIS imagery but it is often evident in the WV imagery where its progress can be traced for up to a day as an expanding 'dark zone' (Smigielski and Ellrod 1985, Young et al 1987, Weldon and Holmes 1991). The precise shape of a WV dark zone varies depending on factors such as the shape of the trough-ridge system.

2. Relationship of the dry intrusion to moist ascending air

The dry intrusion can be visualised to a zeroth order approximation as one half of a rather symmetrical transverse circulation as shown in Figure 3. As the descending dry-intrusion air fans out behind the surface cold front, the ascending moist flow fans out in the middle or upper troposphere behind a front-like boundary corresponding to the convex outer edge of the cloud head. The two flows intertwine in the region of the cyclone centre (L) where part of the dry intrusion (with low θ_w) overrides part of the moist flow (high θ_w). The leading edge of the overrunning part of the dry intrusion constitutes an upper- or middle-level cold θ_w-front (moisture front), often referred to simply as an upper cold front (UCF). Depending on the magnitude of the ambient stretching deformation, the two fan-shaped flows may be elongated parallel to the cold front more or less than in Figure 3.

Analysts concerned with interpreting satellite imagery from research (Browning and Roberts 1994) and operational forecasting perspectives (Bader et al 1995) have refined the model in Figure 3. They have concentrated on defining the moist flows in terms of so-called conveyor-belt flows. Figure 4 shows the cloud-head flow in Figure 3 to be made up of a cold-conveyor-belt (CCB) flow originating ahead of the surface warm front. This is overridden by a flow originating from the warm sector, referred to as a secondary warm conveyor belt (W2). It is the latter, high θ_w , flow that is itself overrun by the low-θ_w dry intrusion to produce the potential instability responsible for the convective events as discussed in Section 4.

Also shown in Figure 4 is a major flow of high-θ_w air labelled W1. This is the primary warm conveyor belt (WCB) responsible for the polar-front cloud-band which for simplicity was omitted from Figure 3. This flow deepens as it travels towards, and eventually rises above, the warm frontal zone. Its left-hand boundary is often sharply defined in the satellite imagery where it encounters dry-intrusion air undercutting it, sometimes to a greater degree than shown in Figure 4.

The overall situation depicted in Figure 4 corresponds to the frontal-fracture stage of Shapiro and Keysers' (1990) cyclone life-cycle model. However, the precise configuration of the principal flows depends on the larger-scale ambient flow (Bader et al 1995). We shall confine ourselves here to drawing a contrast between two major archetypes identified by Young (1994). The first of these, corresponding to Figure 4, occurs in association with confluent troughs. The second common archetype, shown in Figure 5, occurs in association with diffluent troughs. Here the secondary WCB extends to a greater distance away from the primary WCB before rising in the cloud head, and it is overrun by dry-intrusion air over a broader front.

3. Relationship of the dry intrusion to the cold frontal structure

Figure 6 shows a Limited Area Model portrayal of the dry intrusion for a case conforming to the diffluent-trough archetype in Figure 5. Over the previous 9-hour period the cloud head had emerged polewards from beneath the polar-front cloud-band. Figure 6 depicts the system - relative flow on the 20°C isentropic surface which the cross-section in (b) shows to be in the middle of the dry intrusion. The dry intrusion is characterised by air

with relatively high PV emanating from the region of a tropopause fold, although at the resolution of the LAM most of the PV is between 0.5 and 2 PV units rather than exhibiting values of > 2 PV units typical of stratospheric air. Within the limitations of the steady-state assumption, Figure 6(a) shows that the air in the dry intrusion is systematically descending towards the position of the surface cold front (SCF).

When a dry intrusion reaches the SCF it can interact with the high-θ_w WCB air ahead of it in two distinct ways, giving different frontal archetypes. The detailed analysis of Browning and Roberts (1996) for this case shows that the transition between the two archetypes occurred close to where the section AB crosses the front. Using terminology introduced by Bergeron (1937) and applied by Sansom (1951), the cold front was a kata-front to the northeast of AB and an ana-front to the southwest.

Sections normal to the SCF through idealised kata- and ana-cold fronts are sketched in Figures 7(a) and (c), respectively. In the ana-cold front most of the dry-intrusion air undercuts an extrusion of WCB air as part of a well-developed transverse circulation which generates a wide rainband. In the kata-cold front the dry-intrusion air overruns the WCB air for a distance that varies from tens to perhaps 200 kilometres; it then terminates as a UCF where the WCB deepens abruptly and often convectively (not shown in Figure 7(a)). This corresponds to the split cold-front model of Browning and Monk (1982). The split upper and surface cold fronts are plotted separately in the kata-cold frontal region of Figure 6(a).

Given detailed observations it is possible to show that kata- and ana-cold fronts are extremes in a spectrum of frontal structures. Figure 7(b) shows an intermediate structure corresponding to an early stage in the evolution of an ana-cold front from a kata-cold front.

4. Development of potential instability associated with dry intrusions

When a dry intrusion with its relatively low θ_w overruns warm-conveyor-belt air at a kata-cold front, potential instability is generated. This may eventually be released as convection after sufficient lifting has occurred. The mode of development of the region of potential instability, and indeed the formation of the kata-cold front itself, can be visualised by considering the way in which the θ_w-field evolves during overrunning (Figure 8).

Figure 8 shows a time-series of snapshots from a mesoscale model depicting the evolution of the θ_w-field during the deepening of a surface low (at location L). For simplicity a single θ_w-surface, corresponding to the middle of the frontal zone, is analysed where it intersects the 950 and 700 mb levels. The sequence shows how the surface winds up with time. This is associated with the field of rotation shown in the larger-area analysis on the right of Figure 8. The system-relative winds shown are for the 700 mb level where the rotation tends to be greatest. Lower down, the θ_w-surface rotates less, although it remains to be established to what extent this is due to differential rotation or to diabatic warming closer to the ground. In any case, this kind of *effective* differential rotation with height is commonly observed and it leads to a localised region of overrunning. Figure 8 shows that the region of maximum overrunning coincides with the leading edge of the dry intrusion.

Figure 9 shows a model-derived vertical section through the region of overrunning for a case in which severe thunderstorms were triggered. The dry intrusion with its high PV can be seen (Figure 9(a)) slicing into a region of high relative humidity and cloud. The corresponding region is seen (in Figure 9(b)) to be associated with low-θ_w air (equivalent potential temperature is plotted in the figure) overrunning high-θ_w air in the boundary layer. The severe thunderstorms occurred at the leading edge of the dry intrusion where the model's convective parametrization was in fact being activated as shown by the column of asterisks in Figure 9(b).

5. Potential vorticity fine-structure within dry intrusions

We discussed in the Introduction how part of a dry intrusion is likely to be characterised by high PV brought down from the upstream tropopause. In most cyclones stratospheric air descends a little but does not penetrate as far as the lower troposphere; however, occasionally, as in the case depicted in Figure 9, it does. Figure 9(a) shows pockets of air with PV=2 that were brought down within part of the dry intrusion to very low levels. Here they come into close proximity with regions of high PV in the moist air, caused by latent heat release.

The question arises as to the dynamical significance of the stratospheric air descending to such low levels. A possible answer is provided by Figure 8 where the bold line connecting the numbers 500 to 700 marks the axis of the tropopause fold (strictly PV=1.5 rather than 2 units). A cross-section (not depicted) shows that this was a thin filament only 30 to 100 km wide, rather like that in Figure 9 (a). It is evident from Figure 8 that the location of the PV filament does not coincide with the centre of rotation. Indeed, it may be that the filament is so small a feature that to a first approximation it can be considered to be passively advected within the dry-intrusion region by a circulation induced by the larger-scale PV distribution. The thin PV filament extends beneath a larger-scale downward bulge in the PV=2 surface near 500 mb and it is likely that this is dynamically the more significant upper-level feature where cyclogenesis is concerned. WV imagery is highly responsive to dry air at such levels and above (Weldon and Holmes 1991) and this is what underpins the belief that it can be used as a proxy for identifying and bogussing errors in NWP model-derived PV (Thorpe and Demirtas 1996).

6. Dry intrusions in the absence of strong low-level forcing.

Dry intrusions are a manifestation of upper-level forcing of cyclogenesis associated with a positive upper-level PV anomaly (or upper-level trough, or jet streak, depending on one's point of view). Forcing of cyclogenesis also occurs at lower levels in association with PV anomalies within the moist air. In rapidly developing cyclones, forcing usually occurs at both levels and the effects tend to couple as the high-level PV-maximum overruns the low-level baroclinic zone (Hoskins et al 1985). Often, however, strong upper-level forcing occurs in the absence of major low-level forcing. The result may be a relatively weak surface cyclone but the dry intrusion can still produce substantial overrunning and convective weather events.

7. Applications to forecasting

The identification of dry intrusions from WV imagery is useful in 2 ways for forecasting. First, it helps the forecaster understand what is happening on the mesoscale and to anticipate what may happen over the period of a nowcast. This is especially valuable in situations of rapid cyclogenesis and/or convective activity when local warnings of hazardous weather may need to be issued. Secondly, it can be used to validate and bogus a NWP model. The bogussing can be quite effective because of the link between (parts of) dry intrusions and high PV. At present this is being done subjectively as described by Mansfield (1994). Current research at the JCMM is directed at automating this procedure.

References

Bader, M.J., Forbes, G.S., Grant, J.R., Lilley, R.B.E. & Waters, A.J. (1995). Images in weather forecasting. Cambridge University Press, 499 pp

Bergeron, T. (1937). On the physics of fronts.*Bull.Am.Meteorol.Soc.*, **18**, 265 - 275.

Browning, K.A., Ballard, S.P. & Davitt, C.S.A. (1997). High-resolution analysis of frontal fracture. *Mon.Weather Rev.*, **124**, In press.

Browning, K.A., Clough, S.A., Davitt, C.S.A., Roberts, N.M., Hewson, T.D. & Healey, P.G.W. (1995). Observations of the mesoscale sub-structure in the cold air of a developing frontal cyclone, *Q.J.R.Meteorol.Soc.*, **121**, 1229 - 1254.

Browning, K.A. & Golding, B.W. (1995). Mesoscale aspects of a dry intrusion within a vigorous cyclone, *Q.J.R.Meteorol.Soc.*, **121**, 463 - 493.

Browning, K.A. & Monk, G.A. (1982). A simple model for the synoptic analysis of cold fronts. *Q.J.R.Meteorol.Soc.*, **108**, 435 - 452.

Browning, K.A. & Roberts, N.M. (1994). Structure of a frontal cyclone. *Q.J.R.Meteorol. Soc.*, **120**, 1535 - 1557.

Browning, K.A. & Roberts, N.M. (1996). Variation of frontal and precipitation structure along a cold front. *Q.J.R.Meteorol.Soc.*, **122**, 1845-1872.

Danielsen, E.F. (1964). Project Springfield Report. Defense Atomic Support Agency, Washington D.C. 20301, DASA 1517 (NTIS # AD - 607980), 97 pp.

Hewson, T.D. (1997). Article submitted to *Meteorological Applications.*

Hoskins, B.J., McIntyre, M.E. & Robertson, A.W. (1985). On the use and significance of isentropic potential vorticity maps. *Q.J.R.Meteorol.Soc.*, **111**, 877 - 946.

Mansfield, D. (1994). The use of potential vorticity in forecasting cyclones : operational aspects. In *The Life Cycles of Extratropical Cyclones. Vol III, Proc. International Symposium, 27 June - 1 July 1994, Bergen,* pp. 326 - 331.

Sansom, H.W. (1951). A study of cold fronts over the British Isles. *Q.J.R.Meteorol.Soc.*, **77**, 96 -120.

Shapiro, M.A. & Keyser, D. (1990). Fronts, jet streams and the tropopause. In *Extratropical cyclones. The Erik Palmén Memorial Volume. Am.Meteorol.Soc.*, pp. 167 - 191.

Smigielski, F.J. & Ellrod, G.P. (1985). Surface cyclogenesis as indicated by satellite imagery. In *NOAA Tech. Memo. NESDIS 9,* pp. 1 - 29

Thorncroft. C.D., Hoskins, B.J. & McIntyre, M.E. (1993). Two paradigms of baroclinic-wave life-cycle behaviour. *Q.J.R.Meteorol,Soc.*, **119**, 17 - 55.

Thorpe, A.J. & Demirtas, M. (1996). Paper submitted to Nature.

Weldon, R.B. & Holmes, S.J. (1991). Water vapor imagery, interpretation and applications to weather analysis and forecasting. *NOAA Tech. Report NESDIS 57*, 213 pp.

Wernli, J.M. (1995). Lagrangian perspective of extratropical cyclogenesis, PhD Dissertation No 11016, Swiss Federal Inst. of Tech., Zürich, 157 pp.

Young, M.V. (1994). A classification scheme for cyclone life-cycles : applications in analysis and short-period forecasting. In *The Life Cycles of Extratropical Cyclones, Vol III, Proc. International Symposium, 27 June - 1 July 1994, Bergen,* pp. 380-385.

Young, M.V., Monk, G.A. & Browning, K.A. (1987). Interpretation of satellite imagery of a rapidly deepening cyclone. *Q.J.R.Meteorol.Soc.*, **113**, 1089 -1115.

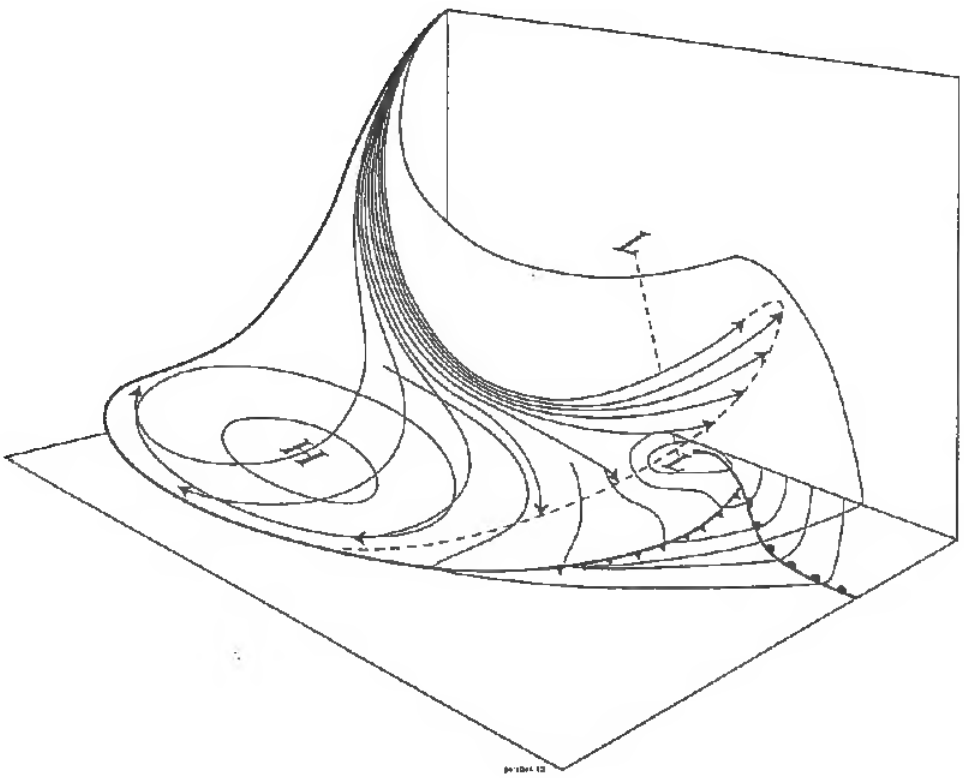

Figure 1. 3-D representation of the dry-intrusion flow . Arrows are trajectories of air originating from a small region near the tropopause, drawn within a curved isentropic surface. These trajectories come close to the ground in the left part of the diagram but not in the right-hand part, where they overrun the surface fronts (Danielsen 1964).

Figure 2. Meteosat infra-red image for 2100 UTC, 7 October 1995 showing a dry slot sandwiched between polar-front cloud-band to the southeast and cloud head to the northwest. Superimposed is the 3-hour forecast from the operational Met Office limited area model as produced routinely using the method outlined by Hewson (1997). White lines are sea-level isobars. Black lines are objectively derived fronts. Surface fronts are shown solid and upper (600 mb) fronts are dotted, thereby enabling the slope of the fronts to be visualized in relation to the cloud pattern.

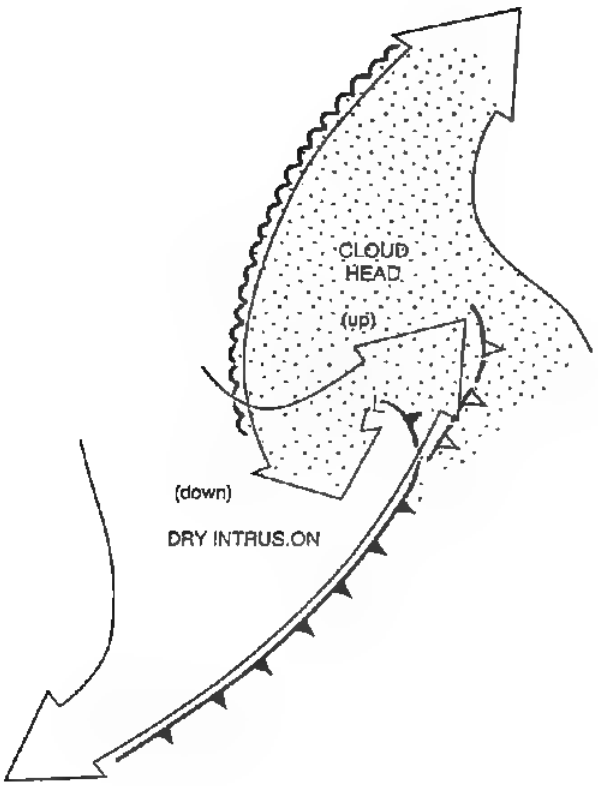

Figure 3. Highly idealized conceptual model showing the intertwining around the cyclone centre (L) of two rather symmetrical flows : the dry intrusion and a moist flow responsible for the cloud head (originating from both sides of the warm front as clarified in Figure 4). The leading edge of much of the dry intrusion is situated along a surface cold front. Part of the dry intrusion overruns the moist flow to give an upper cold front (open frontal symbols). (After Browning et al 1995)

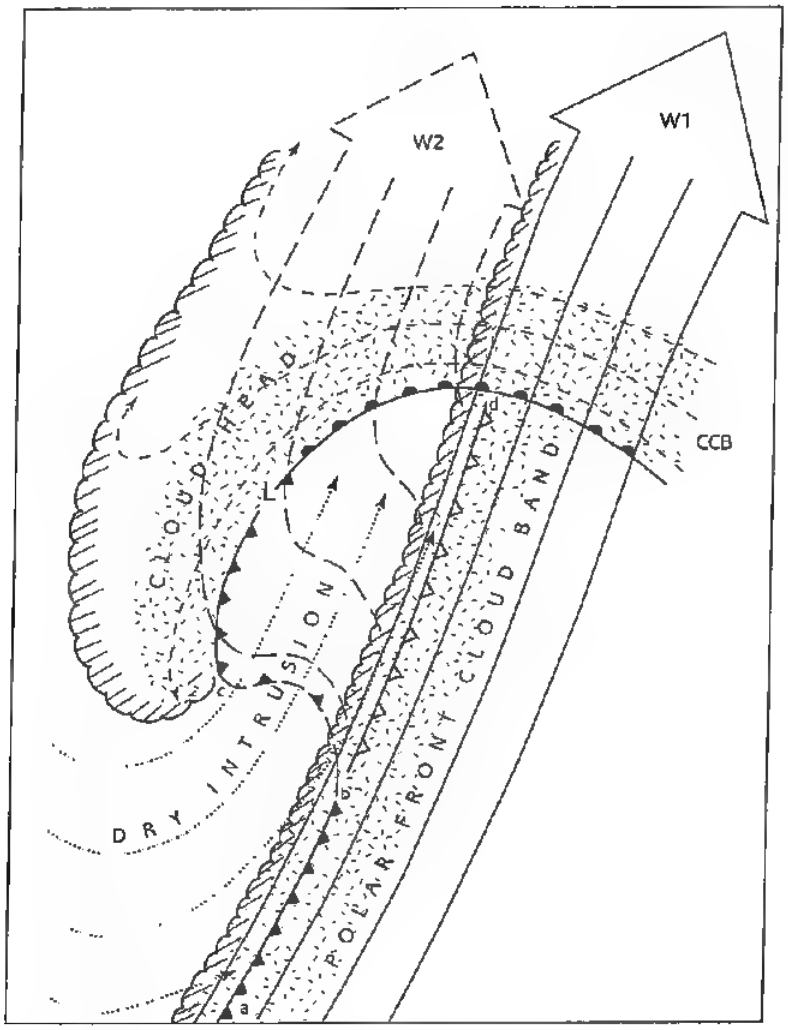

Figure 4 Structure of a developing extratropical cyclone (confluent-flow type). The cyclone centre (L) is travelling towards the top right. The surface warm front is shown conventionally. Part of the bent-back front (cd) is plotted as a cold front with closely-spaced frontal symbols. The main surface cold front (ab) is shown similarly. In between the two sharp surface cold fronts (bc) there is a diffuse surface cold front drawn dashed with widely-spaced frontal symbols.. The cold front drawn with open symbols (bd) is an upper cold θ_w-front (UCF) marking the leading edge of the dry intrusion. Principal airflows, drawn relative to the system, are : the main warm conveyor belt (W1) (solid lines), the secondary warm conveyor belt (W2) (long-dash lines), the cold conveyor belt (CCB) (short-dash lines) and the dry intrusion (dotted lines). The cold-air sides of the main cloud features are drawn scalloped and hatched: the polar-front cloud band is due to W1, and the cloud head is due to the combined effect of W2 and the CCB. Precipitation (stippled areas) reaches the surface along the left side of W1, near the cold fronts, and above the warm frontal zone; precipitation also falls from the inner parts of the cloud head starting at the bent-back front. The two main areas of precipitation are separated by a dry slot where the shallow W2 flow is capped by the dry intrusion. The dry slot is usually characterized by partial shallow cloudiness.

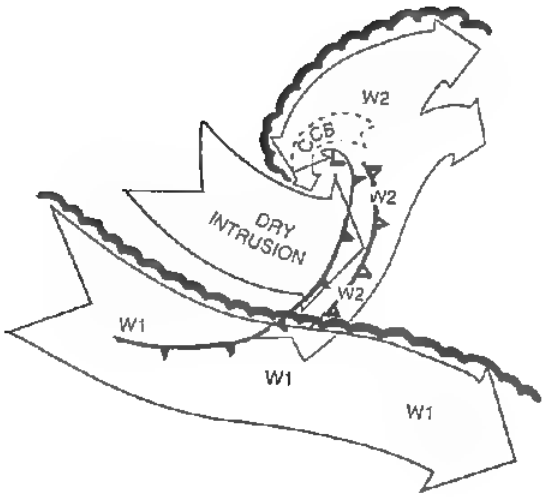

Figure 5. Conceptual model showing system-relative airflow associated with the diffluent-flow type of cyclogenesis. The arrows labelled W1 andW2 are the primary and secondary warm conveyor belts. The dashed arrow, labelled CCB is a cold conveyor belt. The dry intrusion is seen to overrun W2 over a broad region to produce an upper cold front at its leading edge. (After Young 1994).

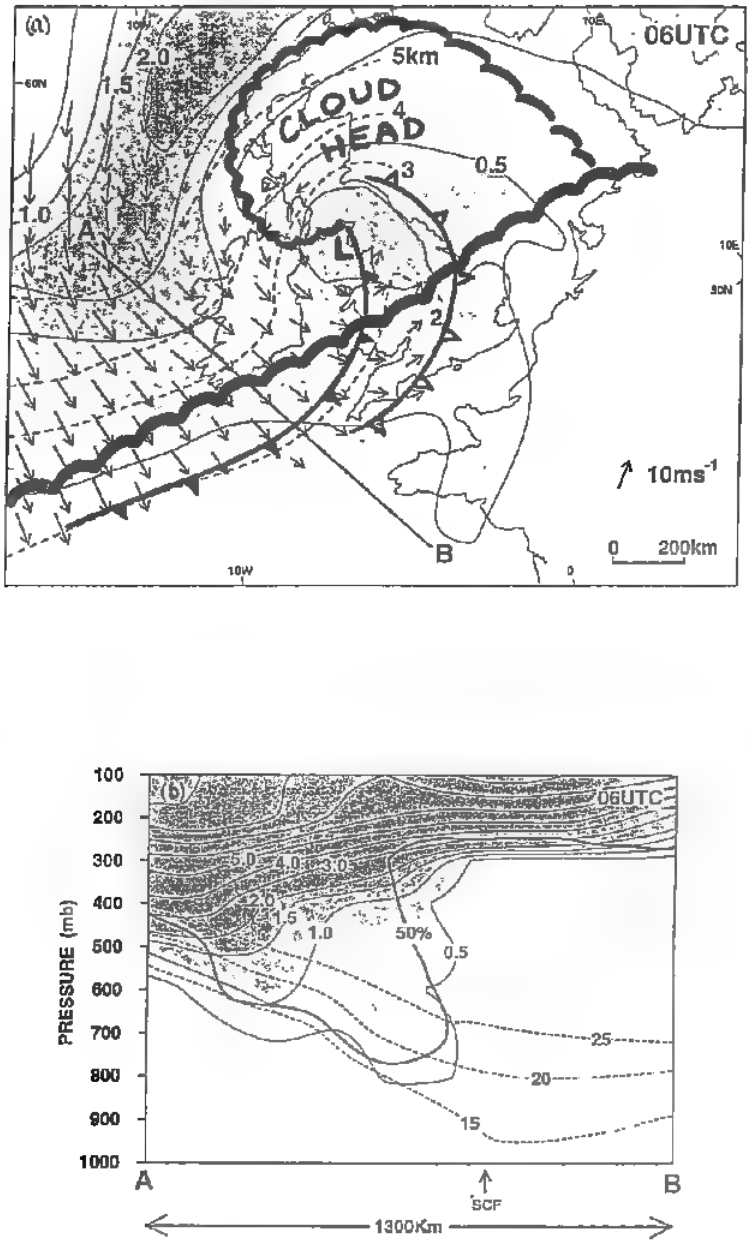

Figure 6. 3-D structure of the dry intrusion associated with a cyclone system at 06 UTC, 8 December 1994, derived from the 00 UTC forecast run of the operational Met. Office limited area model. (a) is a plan view showing the distribution of potential vorticity (solid curves and increasingly dark shading for PV > 0.5, 1.0, 1.5 and 2.0 PVU) and system-relative flow within the θ = 20°C isentropic surface, the height of which is given by dashed curves at 2, 3, 4 and 5 km. Also shown are surface fronts and cloud outlines as in Figure 5. (b) is a cross-section along AB in (a) showing the relationship of the dry intrusion to the PV distribution in the vertical. PV is depicted as in (a). The thick curve shows the downward protrusion of air with relative humidity less than 50%. Dashed curves in (b) show the 20^0 isentrope and isentropes 5° on either side. (After Browning and Roberts 1996).

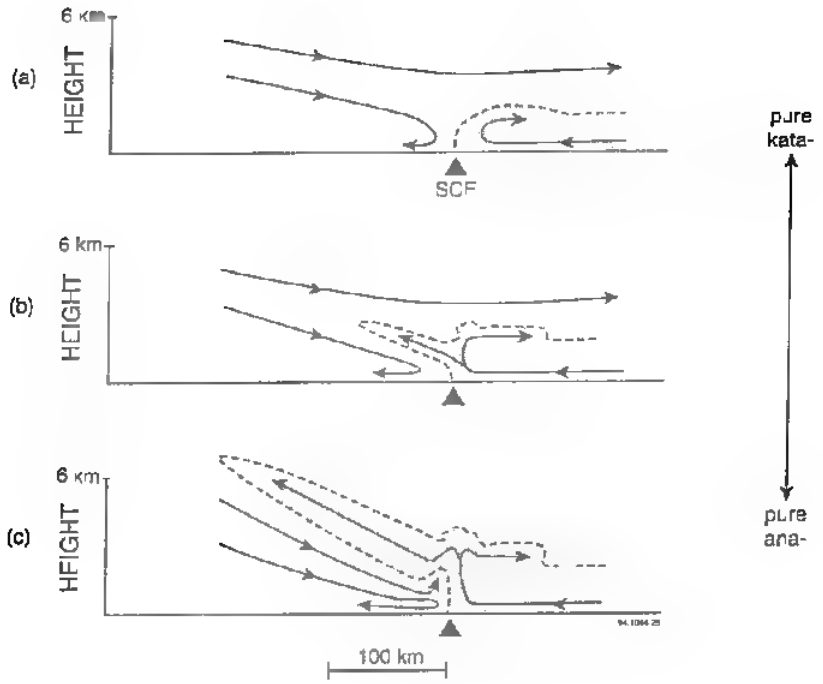

Figure 7. Schematic cross-sectional representations of the spectrum of cold-front types, ranging from a pure kata-cold front (a) to a pure ana-cold front (c). Arrows show transverse flow relative to the front. Stippled shading bounded by dashed lines represents boundary-layer air or extruded boundary-layer air.

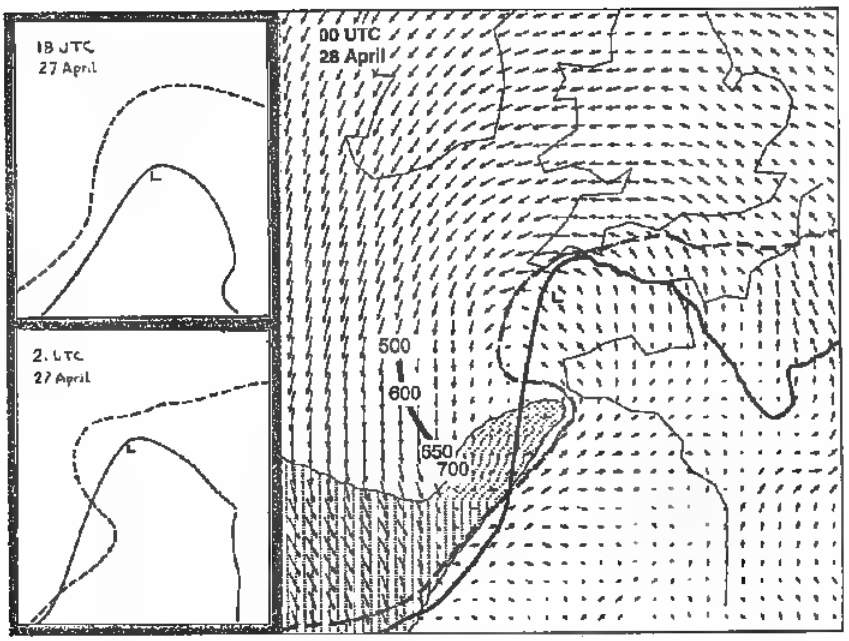

Figure 8. Output from the Met. Office mesoscale model on 27/28 April 1992 depicting the winding up of the θ_w = 9°C surface under the influence of cyclonic rotation. (Left side and main diagram): Three-hourly sequence from 18 UTC 27 April (T+0) to 00 UTC 28 April (T+6) showing the 9° surface at 700 mb (dashed) and 950 mb (solid). (Main diagram): System-relative flow and extent of dry air (relative humidity 30%) at 700 mb plotted together with the $\theta_w = 9^0$C surface for 00 UTC.. Numbers show positions of the axis of the tropopause fold between the 500- and 700-mb levels. The main diagram is plotted to the same scale as those on the left-side but it covers a larger area. (After Browning et al 1997)

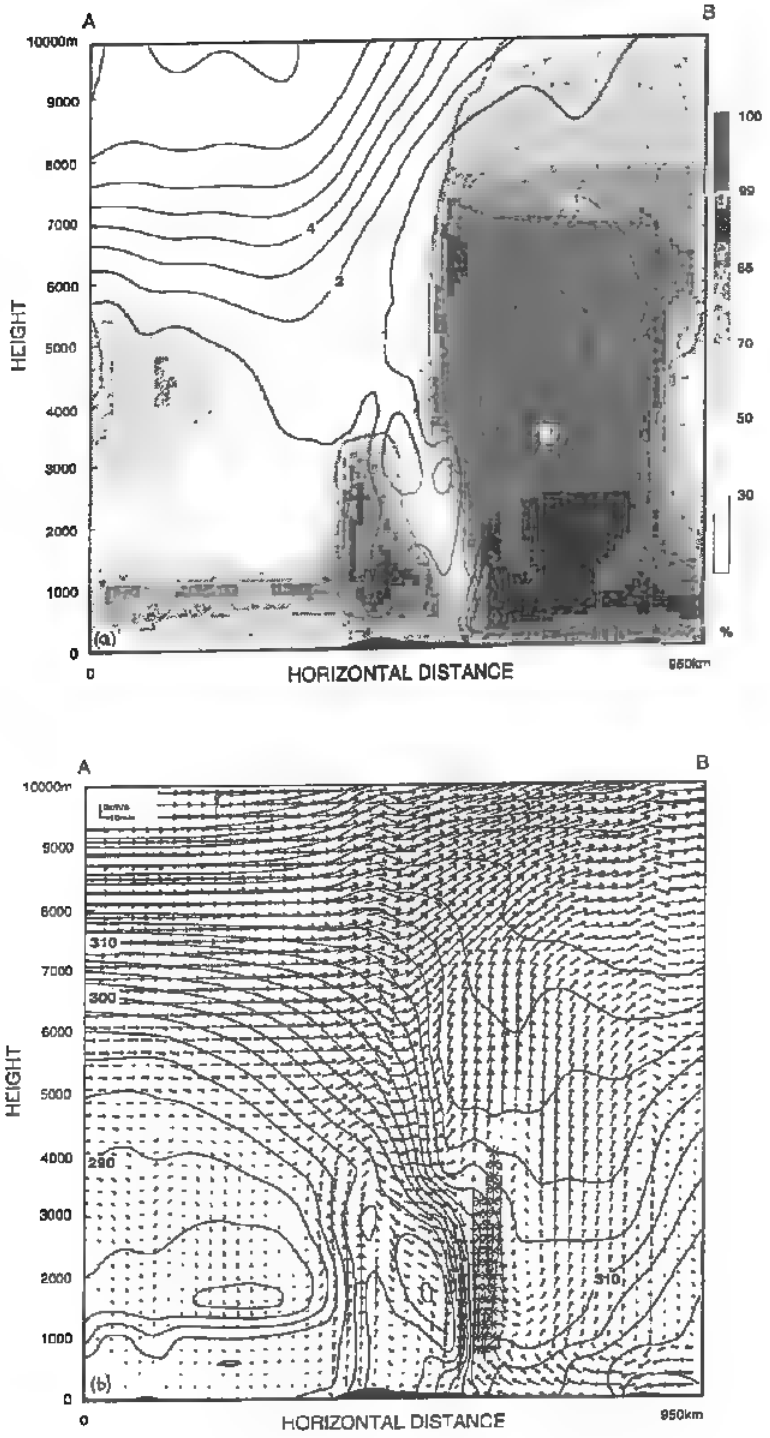

Figure 9. Forecast cross-sections through a dry intrusion obtained from the Met. Office mesoscale model at 18 UTC, 12 November 1991. (a) shows relative humidity with respect to water (shading), the cloud boundary (dashed contours) and potential vorticity (solid contours at intervals of 1 PV unit). (b) shows the equivalent potential temperature (K) overlaid on the system-relative flow in the plane of the section. Regions experiencing parametrized release of potential instability are indicated by asterisks.

CURRENT JCMM INTERNAL REPORTS

This series of JCMM Internal Reports, initiated in 1993, contains unpublished reports and also versions of articles submitted for publication. The complete set of Internal Reports is available from the National Meteorological Library on loan, if required.

1. **Research strategy and programme**
   K A Browning et al
   January 1993

2. **The GEWEX Cloud System Study (GCSS)**
   GEWEX Cloud System Science Team
   January 1993

3. **Evolution of a mesoscale upper tropospheric vorticity maximum and comma cloud from a cloud-free two dimensional potential vorticity anomaly**
   K A Browning
   January 1993

4. **The global energy and water cycle**
   K A Browning
   July 1993

5. **Structure of a midlatitude cyclone before occlusion**
   K A Browning and N Roberts
   July 1993

6. **Developments in systems and tools for weather forecasting**
   K A Browning and G Szejwach
   July 1993

7. **Diagnostic study of a narrow cold frontal rainband and severe winds associated with a stratospheric intrusion**
   K A Browning and R Reynolds
   August 1993

8. **Survey of perceived priority issues in the parametrizations of cloud-related processes in GCMs**
   K A Browning
   September 1993

9. **The effect of rain on longwave radiation**
   I Dharssi
   September 1993

10. **Cloud microphysical processes - a description of the parametrization used in the large eddy model**
    H Swann
    October 1993

11. **An appreciation of the meteorological research of Ernst Kleinschmidt**
    A J Thorpe
    May 1992

12. **Potential vorticity of flow along the Alps**
    A J Thorpe, H Volkert and Dietrich Heimann
    August 1992

13. **The representation of fronts**
    A J Thorpe
    January 1993

29. **Mesoscale effects of a dry intrusion within a vigorous cyclone**
K A Browning and B W Golding
April 1994

30. **GEWEX Cloud System Study, Science Plan**
May 1994

31. **Parametrization of momentum transport by convectively generated gravity waves**
R Kershaw
May 1994

32. **Mesoscale Modelling Newsletter No 5**
May 1994

33. **Observations of the mesoscale sub-structure in the cold air of a developing frontal cyclone**
K A Browning, S A Clough, C S A Davitt, N M Roberts and T D Hewson
May 1994

34. **Longwave radiative forcing of a simulated tropical squall line**
Imtiaz Dharssi
July 1994

35. **On the nature of the convective circulation at a kata-cold front**
K A Browning
September 1994

36. **Collective preprints of papers submitted to the COST-75 International Seminar on Advanced Weather Radar Systems, Brussels, 20-23 September 1994**
November 1994

37. **Use of satellite imagery to diagnose events leading to frontal thunderstorms: Parts I and II of a case study**
K A Browning and N M Roberts
November 1994

38. **The role of spaceborne millimetre-wave radar in the global monitoring of ice cloud**
P R A Brown, A J Illingworth, A J Heymsfield, G M McFarquhar, K A Browning and M Gosset
December 1994

39. **Potential vorticity inversion**
Michal Ziemianski
October 1994

40. **Theory of mature tropical cyclones; a comparison between Kleinschmidt (1951) and Emanuel (1986)**
Suzanne L Gray
December 1994

41. **Dispersion and removal of pollutants during the passage of an atmospheric frontal system**
N R Gimson
December 1994

42. **The role of snow sublimation in frontogenesis**
D J Parker and A J Thorpe
December 1994

43. **Potential vorticity and the electrostatics Analogy: Ertel-Rossby formulation**
A J Thorpe and C H Bishop
December 1994

44. **Mesoscale aspect of extratropical cyclones: an observational perspective**
K A Browning
January 1995

61. **The role of the environmental flow in the development of secondary frontal cyclones**
I A Renfrew, A J Thorpe and A Joly
June 1996

62. **Consequences of the geostrophic momentum approximation on barotropic instability**
S Malardel, A J Thorpe and A Joly
June 1996

63. **Contributions to the AMS/RMS Conference on Mesoscale Processes**
Reading, 9-13 September 1996

64. **Vorticity and potential vorticity in stratified flows interacting with an isolated obstacle**
Jorge A Gutiérrez and A J Thorpe
September 1996

65. **Triple point development: two case studies**
Douglas Parker
September 1996

66. **Radar observations of wind-shear splitting within evolving atmospheric Kelvin-Helmholtz billows**
D Chapman and K A Browning
April 1997

67. **Cold frontal structure derived from radar wind profilers**
K A Browning, D Jerrett, J Nash, T Oakley and N M Roberts
May 1997

Met Office Joint Centre for Mesoscale Meteorology Department of Meteorology
University of Reading PO Box 243 Reading RG6 6BB United Kingdom
Tel: +44 (0)118 931 8425 Fax: +44 (0)118 931 8791
www.metoffice.com